

A Novel Texture Feature Based on Fourier Transform for Building Damage Recognition from PolSAR Data

Wei Zhai,^{1,2,3} Yixin Bi,^{3*} Xiaoqing Wang,² and Xiang Wang⁴

¹Lanzhou Institute of Geotechnique and Earthquake, China Earthquake Administration,
No. 450 Donggang West Road, Chengguan District, Lanzhou 730000, China

²Institute of Earthquake Forecasting, China Earthquake Administration,
No. 63, Fuxing Road, Haidian District, Beijing 100036, China

³Faculty of Computing, Engineering and the Built Environment, Ulster University,
York St, Belfast, Northern Ireland, BT15 1ED, United Kingdom

⁴Hebei Seismological Station, Hebei Earthquake Agency,
No. 262 Huazhong Road, Yuhua District, Shijiazhuang 050021, China

(Received February 14, 2023; accepted September 5, 2023)

Keywords: SAR, Fourier transform, texture feature, building damage, earthquake

Building collapse arising from destructive earthquakes is often the primary cause of casualties and economic loss. Building damage assessment is one of the top priorities in earthquake emergency work. Quad-polarimetric synthetic aperture radar (PolSAR) data not only have the advantages of radar imaging being neither exposed to sunlight nor blocked by clouds, but also contain the most abundant information of the four polarimetric channels. Only using conventional polarimetric decomposition methods may lead to overestimations of the number of collapsed buildings and the exaggeration of the degree of earthquake damage. We proposed a parameter called the sector texture feature of the Fourier amplitude spectrum (STFFAS) to describe frequency-domain texture features based on the Fourier amplitude spectrum in order to solve the overestimation of earthquake building damage. In addition, we proposed a scheme to recognize building earthquake damage using only a single post-earthquake PolSAR image combined with STFFAS and the improved Yamaguchi four-component decomposition method. The 4.14 Ms7.1 Yushu earthquake that occurred in Yushu County, China, in 2010 is taken as the experimental case. Compared with conventional polarimetric decomposition methods, this method successfully separated 70.18% of standing buildings from the ground objects mixed with collapsed buildings, thus significantly improving the extraction accuracy and reliability of building earthquake damage information.

1. Introduction

In the recent decade, earthquakes have occurred frequently around the world, causing huge losses to human life and property.⁽¹⁾ In urban areas, earthquake casualties are mainly caused by collapsed buildings. During search and rescue operations for people buried in the rubble, the sooner the information about the collapse of buildings is obtained, the higher the probability of

*Corresponding author: e-mail: y.bi@ulster.ac.uk
<https://doi.org/10.18494/SAM4346>

human survival. Therefore, fast and accurate statistics on the distribution of collapsed buildings in the earthquake-stricken area is a top priority after an earthquake as well as a guideline for developing other earthquake emergency plans. The main method of traditional earthquake damage information acquisition is the door-to-door field survey. Although this method has a high reliability of information acquisition, it often has a large workload and low efficiency when carried out in a large area. Remote sensing technology enables the quick monitoring of disasters on a large scale and has become an important means of earthquake emergency response and post-earthquake damage assessment. Earthquakes often occur at night or are accompanied by severe weather conditions, such as overcast, rain and snow, making optical remote sensing ineffective. However, radar waves are not affected by sunlight and can pass through thick clouds to obtain information about the disaster areas isolated from the outside world. Synthetic aperture radar (SAR) remote sensing technology can achieve effective ground target imaging under any weather or climate conditions. Therefore, the use of radar remote sensing for post-earthquake disaster monitoring seems more secure. In the past, multitemporal SAR data were collected before and after an earthquake, and the differences between the pre- and post-event data were used to identify the disaster site. However, the collection of pre-earthquake SAR data is time-consuming and labor-intensive, and pre-earthquake data of some remote areas are not archived. In order to save time and labor, we use only post-earthquake single-temporal SAR data to recognize building earthquake damage in the disaster area. In this way, multitemporal data registration can also be avoided. Quad-polarimetric SAR (PolSAR) data contain considerably more information than do single-polarimetric and dual-polarimetric SAR data since PolSAR has HH, HV, VH and VV polarimetric channels, where H indicates horizontal polarization and V indicates vertical polarization. Therefore, when only post-earthquake single-scene SAR images are used for earthquake building damage assessment, we adopt PolSAR images as data sources to achieve a higher earthquake damage recognition accuracy and highly reliable earthquake damage assessment results.

As PolSAR data sources are becoming increasingly available, many scholars and institutions have applied PolSAR to post-earthquake damage recognition because of the excellent performance of PolSAR in recognizing ground objects.⁽²⁾ Since PolSAR data sources are challenging to obtain in some remote areas and there are no pre-earthquake archived data, together with the fact that the information contained in PolSAR data is sufficient for single-temporal SAR image earthquake damage recognition, a continuously increasing number of scholars have begun to use only post-earthquake single-scene PolSAR data to recognize building earthquake damage in recent years.^(3–4) Experiments have proved that recognition results obtained from a single post-earthquake PolSAR image can meet the requirements of accurate and speedy earthquake damage recognition.⁽⁵⁾ The recognition accuracy is at least as good as that when using multitemporal SAR data. Wang *et al.* analyzed the backscattering mechanism of the damaged buildings in airborne multipolarization SAR images.⁽⁶⁾ Li *et al.* proposed a new H- α - ρ method based on the circular polarization correlation coefficient for extracting the spatial distribution of collapsed buildings from RADARSAT-2 fine-mode PolSAR data.⁽⁷⁾ Chen *et al.* presented a modified Freeman decomposition including selective deorientation and surface scattering characteristic parameter constraint, and used the contribution of the double-bounce

component to extract the collapsed building spatial distribution from post-disaster RADARSAT-2 SAR data.⁽⁸⁾ Zhai *et al.* created a novel polarimetric feature parameter, the normalized difference of the dihedral component (NDDC), to evaluate the degree of building damage.⁽⁹⁾ Ji *et al.* proposed a new unsupervised damage assessment method in accordance with four conditions for damaged-building identification.⁽¹⁰⁾ Zhai *et al.* developed two new polarimetric features λ_H and H_λ on the basis of entropy and eigenvalues of a T3 matrix to discriminate five different types of buildings in disaster areas.⁽¹¹⁾ Liu *et al.* established a model based on components obtained by Touzi decomposition for damage assessment mapping in built-up areas.⁽¹²⁾ Zhai *et al.* developed a new polarimetric feature, the variable coefficient of angle domains based on the Fourier amplitude spectrum parameter (CV_AFI) to assess the degree of building earthquake damage.⁽¹³⁾ Miao *et al.* improved the Freeman polarization decomposition method applicable to earthquake-induced building damage identification.⁽¹⁴⁾ Nie *et al.* created a new polarization feature—the maximal power contrast (MaxC) feature—via the optimization of the polarimetric contrast enhancement (OPCE) matching algorithm for identifying collapsed buildings.⁽¹⁵⁾ Texture features are as important as polarimetric features contained in PolSAR data, and in many cases, exhibit even stronger recognition performance than polarimetric features. Bai *et al.* found that the polarimetric features demonstrated poorer performance than texture features in terms of distinguishing between damage categories.⁽¹⁶⁾ Li *et al.* introduced texture parameters of different statistical models to address the problem of confusing collapsed and oriented buildings.⁽¹⁷⁾ Zhai *et al.* proposed the precision-weighted multifeature fusion (PWMF) method to fuse four texture features for collapsed building extraction from PolSAR images.⁽¹⁸⁾ Chen *et al.* proposed a statistical texture feature G0-para arising from the G0 distribution of SAR images to distinguish buildings in complex urban areas after a disaster.⁽¹⁹⁾ In recent years, because of the rapid development of deep learning technology⁽²⁰⁾ and its high-precision recognition advantages,⁽²¹⁾ many scholars are using the convolutional neural network (CNN) algorithm to recognize building earthquake damage information.^(22,23)

In post-earthquake SAR images, the walls of many damaged buildings collapse, resulting in the destruction of the dihedral structures formed by the walls and the ground, making it impossible to attain the double-bounce scattering characteristics of SAR images with a high scattering intensity, causing volume scattering to be dominant over double-bounce scattering. This results in the scattering intensity of collapsed buildings being lower than that of standing buildings. However, a particular phenomenon that some standing buildings are not arranged parallel to the SAR flight path exists in SAR images; such buildings are called obliquely oriented buildings. With the rotation of the polarization basis of obliquely oriented buildings, these buildings are strongly depolarized, and volume scattering is their predominant scattering mechanism, giving a low scattering intensity. Therefore, obliquely oriented and collapsed buildings have similar scattering mechanisms and scattering intensities, so serious mutual confusion exists in SAR images, leading to the overestimation of damaged buildings. To solve this problem, we propose a novel frequency-domain texture feature based on Fourier transform, i.e., the sector texture feature of the Fourier amplitude spectrum (STFFAS). In addition, STFFAS is used to design the building earthquake damage recognition scheme. Experimental results showed that the earthquake damage recognition accuracy can be significantly improved

by using STFFAS proposed in this paper. Our research design and experiment will be introduced in detail below.

2. Methods

2.1 Polarimetric decomposition method

Different scattering components can be obtained by polarimetric decomposition. In post-earthquake PolSAR images, buildings in different states correspond to different scattering components, e.g., some standing buildings that are parallel to the SAR flight path are called parallel standing buildings, and their dominant scattering component is the double-bounce scattering component; therefore, the earthquake damage recognition results of such buildings in earthquake-stricken areas can be directly obtained by polarimetric decomposition. In our work, the buildings that are undamaged and whose dominant scattering component is the volume scattering component are regarded as obliquely oriented buildings. Both collapsed buildings and standing obliquely oriented buildings in earthquake-stricken areas are dominated by the volume scattering component. In our research, we have conducted the polarimetric decomposition of PolSAR data using the improved Yamaguchi four-component decomposition (Y4R) method to recognize standing buildings (including parallel standing and obliquely oriented buildings) in a more complete manner. The Y4R method was proposed by Yamaguchi *et al.* as an improved version of the traditional Yamaguchi four-component decomposition model (Y4O) to increase the building recognition accuracy and recognize obliquely oriented buildings as comprehensively and accurately as possible (for more details on the Y4R method, see Ref. 24).

2.2 STFFAS

Volume scattering components obtained by polarimetric decomposition correspond to obliquely oriented and collapsed buildings. Although they have similar scattering mechanisms and scattering intensities, they exhibit different texture characteristics in PolSAR images. The strength of the Fourier amplitude spectrum of SAR images represents the rate of change in scattering intensity. Obliquely oriented buildings have relatively regular and fine textures, while collapsed buildings have relatively irregular and coarse textures. The differences in the scattering intensities and textures of the two types of buildings can be better reflected with frequency-domain texture features. In our research scheme, STFFAS is applied to classify the two types of buildings in earthquake-stricken areas to improve the over-classification of collapsed buildings and suppress the overcorrection of obliquely oriented buildings. STFFAS can well describe the difference in texture between obliquely oriented and collapsed buildings, and accurately recognize the two types of buildings. As shown in Fig. 1, the STFFAS values of obliquely oriented buildings are greater than those of collapsed buildings, indicating that STFFAS is adequate for recognizing the two types of buildings.

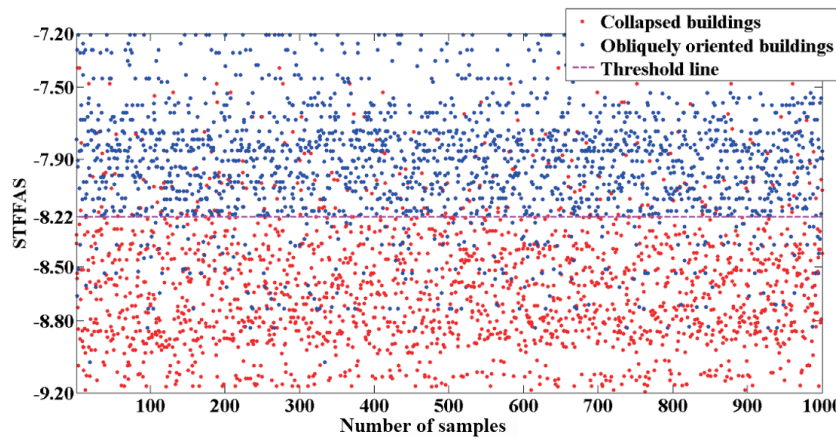


Fig. 1. (Color online) Recognition performance of STFFAS for obliquely oriented and collapsed buildings. Blue and red points in the figure represent 1000 obliquely oriented building samples and 1000 collapsed building samples, respectively.

The STFFAS calculation method is shown in Fig. 2. The total power image of PolSAR data (termed the SPAN image) contains the intensity information of all polarimetric channels. The intensity information in the SPAN image is the most abundant. Therefore, STFFAS of PolSAR data is calculated with the SPAN image. SPAN is calculated as

$$SPAN = HH^2 + HV^2 + VH^2 + VV^2. \quad (1)$$

Traverse the whole-scene SPAN image with the calculation window, calculate the STFFAS values of each calculation window, and obtain the STFFAS data of the PolSAR imagery. The STFFAS calculation method is described below, taking the calculation procedure for STFFAS values in one calculation window as an example.

WI is the SPAN image in the calculation window. There are seven steps in the calculation of STFFAS.

- Step 1. Perform a two-dimensional fast Fourier transform (FFT) on WI to obtain FWI (for details on FFT, refer to Ref. 25).
- Step 2. Calculate the amplitude spectrum of FWI to obtain AFWI.
- Step 3. As shown in Fig. 2, take the center point of the AFWI image as the origin of the coordinates and divide the circle of 2π equally into n parts around the origin of the coordinates, with a vertex angle of $2\pi/n$ radians at the origin coordinates of each equal part. Calculate the sum of AFWI values of all pixels in the i th equal part to obtain AFWI_A_{*i*}. Calculate the sum of the AFWI values of all pixels for each equal part in turn to obtain n AFWI_A_{*i*} values {AFWI_A₁, AFWI_A₂, AFWI_A₃, ..., AFWI_A_{*n*}}.
- Step 4. Calculate the ADFT value of AFWI according to the fourth line of Eq. (2).
- Step 5. As shown in Fig. 2, divide the inscribed circle of AFWI into m rings of the same width by taking the center point of the AFWI image as the origin coordinates. Assuming that each ring has a width of RW, calculate the sum of the AFWI values of all pixels in the j th ring to obtain AFWI_R_{*j*}. Calculate the sum of the AFWI values of all pixels in each ring in turn to obtain m AFWI_R_{*j*} values {AFWI_R₁, AFWI_R₂, AFWI_R₃, ..., AFWI_R_{*m*}}.

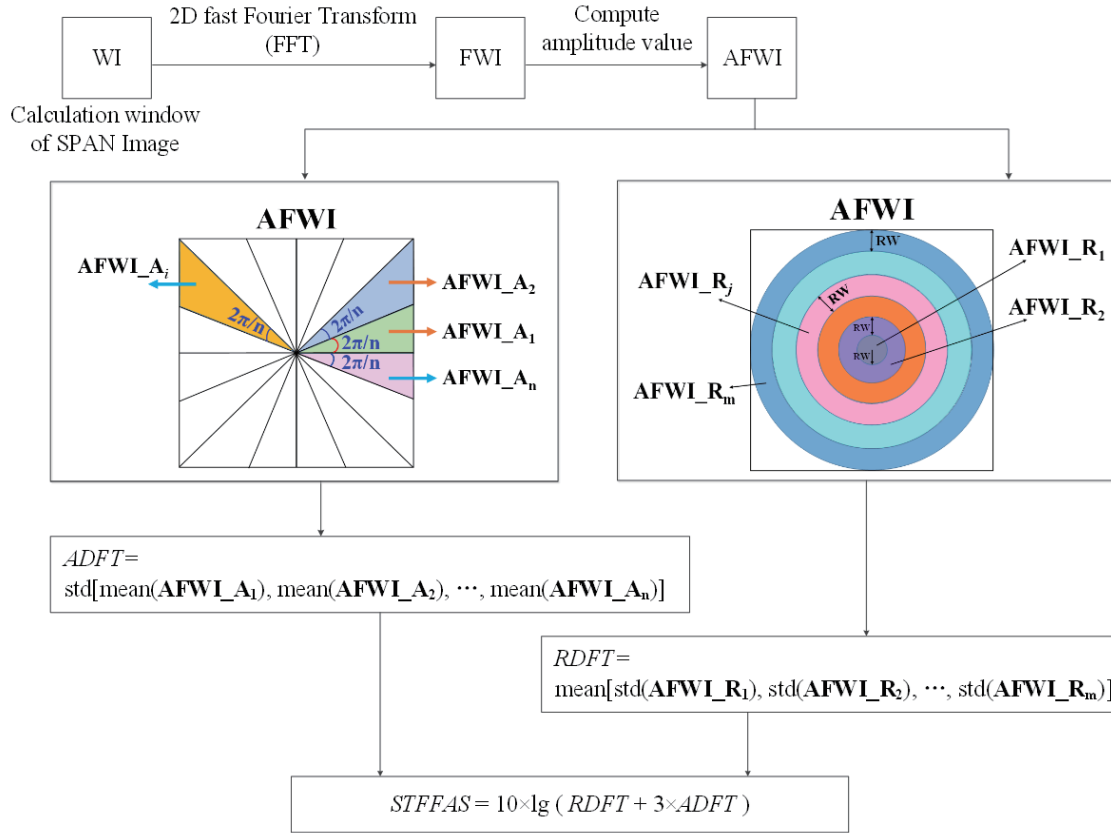


Fig. 2. (Color online) Schematic diagram of STFFAS calculation.

Step 6. Calculate the RDFT value of AFWI according to the fifth line of Eq. (2).

Step 7. Calculate the STFFAS value of WI according to the last line of Eq. (2).

STFFAS can be expressed as

$$WI \subset \text{span image of PolSAR data}$$

$$FWI = \text{FFT}(WI)$$

$$\begin{aligned} AFWI &= \sqrt{[\text{real}(FWI)]^2 + [\text{imag}(FWI)]^2} \\ ADFT &= \text{std}[\text{mean}(AFWI_A_1), \text{mean}(AFWI_A_2), \dots, \text{mean}(AFWI_A_n)] \end{aligned} \quad (2)$$

$$RDFT = \text{mean}[\text{std}(AFWI_R_1), \text{std}(AFWI_R_2), \dots, \text{std}(AFWI_R_m)]$$

$$STFFAS = 10 \times \lg(RDFT + 3 \times ADFT).$$

Here, real and imag represent the real and imaginary parts of a complex number, respectively; mean , std , and \lg represent the calculated mean value, variance, and logarithm to the base 10, respectively.

2.3 Building earthquake damage information extraction procedure

As shown in Fig. 3, the building earthquake damage information extraction procedure includes the following six steps:

- Step 1. Perform a polarimetric decomposition of the PolSAR data by the Y4R method to extract the double-bounce and volume scattering components.
- Step 2. Classify the objects to be recognized in the PolSAR image, whose dominant scattering components correspond to the double-bounce scattering components, as the parallel standing buildings.
- Step 3. Extract the SPAN image from the PolSAR data according to Eq. (1).
- Step 4. Set up an appropriate calculation window, traverse the entire SPAN image by the STFFAS calculation method shown in Fig. 2 and Eq. (2), calculate the STFFAS values, and obtain the entire STFFAS image of the PolSAR data.
- Step 5. Choose an appropriate threshold value for STFFAS, and divide the volume scattering components obtained by polarimetric decomposition into collapsed and obliquely oriented buildings on the basis of the classification rule expressed by Eq. (3). From Fig. 1, the STFFAS values of the obliquely oriented buildings are found to be greater than those of the collapsed buildings. Therefore, the classification rule of STFFAS can be expressed as follows.

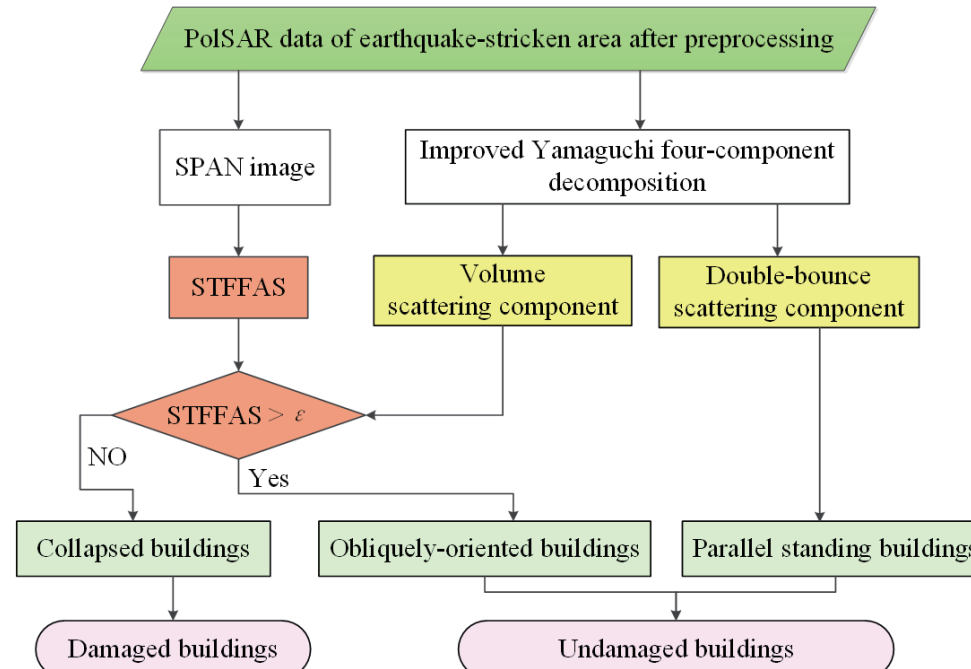
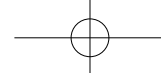


Fig. 3. (Color online) Procedure of extracting damaged and undamaged buildings.



$$\begin{aligned}
 & x \in \text{volume_dominated buildings} \\
 & \quad \text{if } STFFAS \leq \varepsilon \\
 & \quad x \in \text{collapsed buildings} \\
 & \quad \text{if } STFFAS > \varepsilon \\
 & \quad x \in \text{obliquely oriented standing buildings}
 \end{aligned} \tag{3}$$

Here, ε indicates the threshold value for distinguishing between collapsed and obliquely oriented buildings using STFFAS.

- Step 6. Merge the obliquely oriented and parallel standing buildings as undamaged buildings, and define collapsed buildings as damaged buildings.

3. Materials

The case study presented in this paper is based on the 4.14 Ms7.1 Yushu earthquake that occurred in Yushu County, Qinghai Province, China, on April 14, 2010. The epicentre of this earthquake was located at (33.1°N, 96.6°E). Yushu County is at a high altitude where the climate is dry and cold. There is very little vegetation in the urban area. It is sparsely distributed and mostly low vegetation, which has little impact on the identification of buildings in the earthquake-stricken area, so the ground object of vegetation was ignored in this experiment. The mountains surrounding the county were masked using the boundary .shp data of Yushu County, and only earthquake damage information of buildings in the urban area was extracted.

The experimental data was the airborne high-resolution PolSAR image obtained by the Chinese airborne SAR mapping system (SARMapper) one day after the earthquake. Additional information about the PolSAR data used in this experiment is listed in Table 1. Figure 4 presents the 8192×4384 pixel SPAN image of the PolSAR data used to calculate STFFAS. In this experiment, 25000 verification samples were selected for collapsed, obliquely oriented, and parallel standing buildings, using the Google Earth Map and being colored red, blue, and green in Fig. 4, respectively.

4. Results

Damaged and undamaged buildings were extracted from the PolSAR data used in the experiment by the building earthquake damage recognition procedure in Fig. 3. STFFAS was calculated by the method shown in Fig. 2. In this work, the calculation window of STFFAS was

Table 1
Specific information of PolSAR data used in our experiment.

Date	Flight direction	Illumination direction	Incidence angle	Band	Flight altitude (m)	Spatial resolution (m)
15. April 2010	From right to left	Bottom	50°	P	10,079	1 (range); 1 (azimuth)

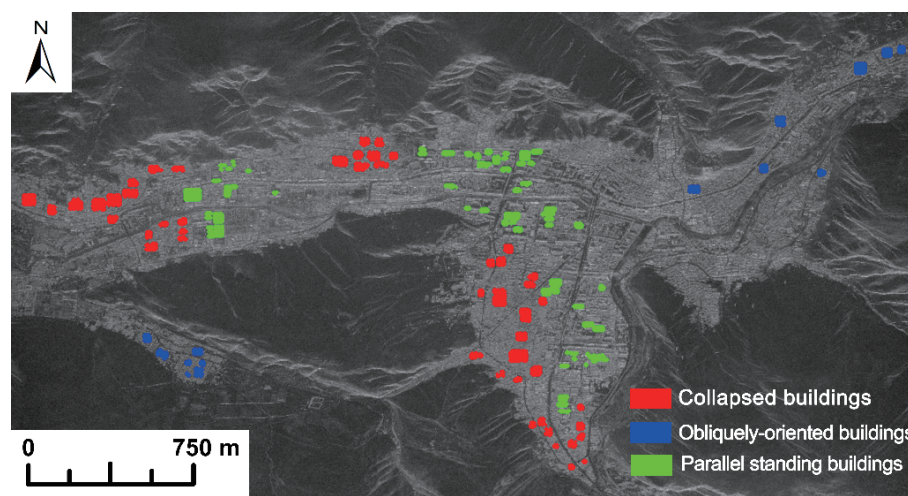
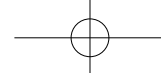


Fig. 4. (Color online) SPAN image of Yushu County marked with the three types of building samples in the earthquake-stricken area.

set to be a square to simplify the experimental calculation. It can be seen from Fig. 5 that the overall accuracy of classification of collapsed buildings, obliquely oriented buildings, and parallel standing buildings is the highest when calculating STFFAS using Eq. (2) with the calculation window size of 57 pixels \times 57 pixels. As shown in Fig. 6, during the calculation of ADFT shown in Fig. 2, when the number n of equally divided angular zones in the circle of 2π in the AFWI image is 36, that is, when the vertex angle of each equal angular zone is $\pi/18$ radians, the overall classification accuracy for the three kinds of buildings is the highest. From Fig. 7, it is seen that during the calculation of RDFT shown in Fig. 2, when the ring width RW is set to 5 pixels, the classification of the three types of buildings has the highest overall accuracy. The number of rings with equal ring width into which the inscribed circle of AFWI is divided is equal to window size/(2 \times RW), that is, $m = \text{window size}/(2 \times \text{RW})$. As can be seen from Fig. 1, there is a clear dividing line between the STFFAS values of the collapsed buildings and those of the obliquely oriented buildings at the STFFAS value of -8.22. The curve shown in Fig. 8 further shows that when the STFFAS value is equal to -8.22, the overall classification accuracy of the three kinds of buildings is the highest. Therefore, in our experiment, when classifying collapsed buildings and obliquely oriented buildings using STFFAS according to Eq. (3), the classification threshold ε is set to -8.22.

The extraction results of building earthquake damage information in this experiment are shown in Fig. 9 for only the buildings with earthquake damage in the urban area after masking the mountains around the urban area using the urban boundary data of Yushu County. With the identified samples of collapsed buildings, obliquely oriented buildings, and parallel standing buildings marked in Fig. 4, the accuracy of the experiment results on building earthquake damage recognition shown in Fig. 9 is evaluated, and the confusion matrix for the accuracy assessment of our experimental results is shown as Table 2. Table 2 shows that the total number of diagonal samples where experimental results are consistent with the reference samples accounted for 81.3% of the total samples. Therefore, the overall correct recognition accuracy of the three kinds of buildings in the research area using our proposed method reached 81.3%.

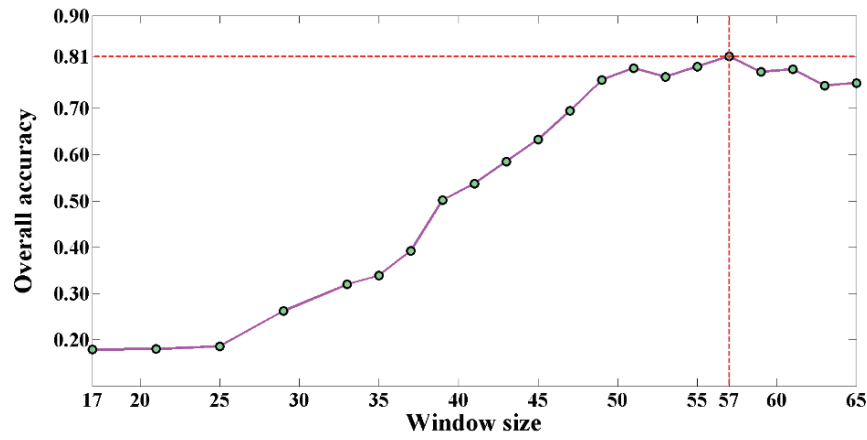


Fig. 5. (Color online) Selection of STFFAS calculation window.

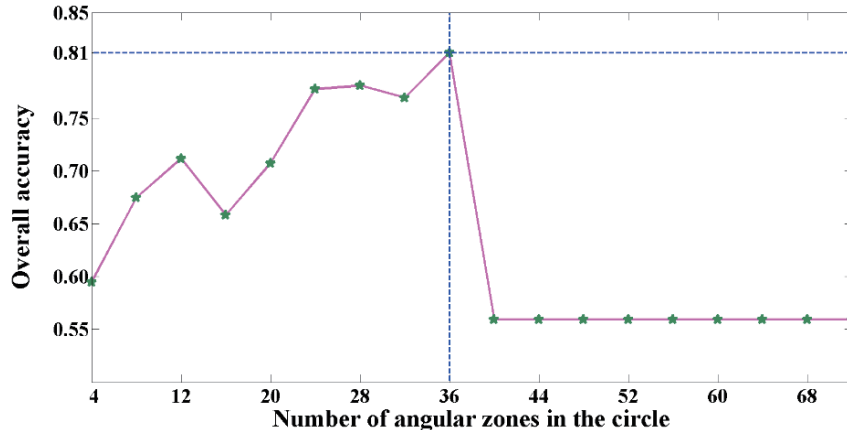


Fig. 6. (Color online) Decision for the number of angular zones with same vertex angle in the circle of 2π of AFWI shown in Fig. 2.

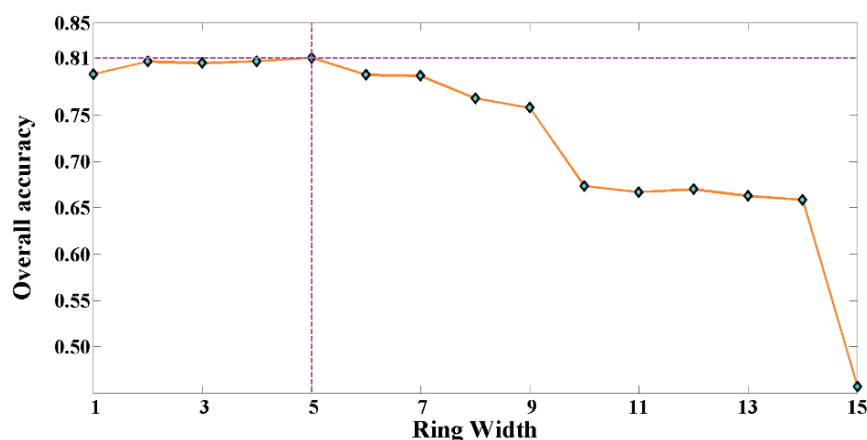


Fig. 7. (Color online) Selection for the number of rings with same width in the inscribed circle of AFWI shown in Fig. 2.

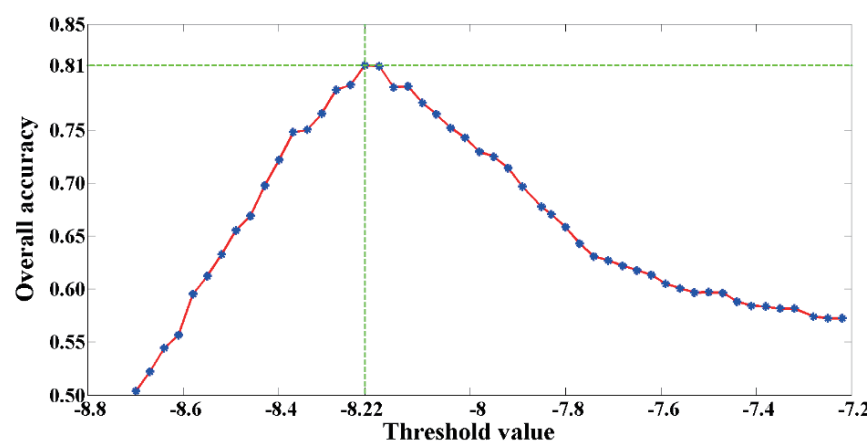


Fig. 8. (Color online) Decision for the threshold value of STFFAS.

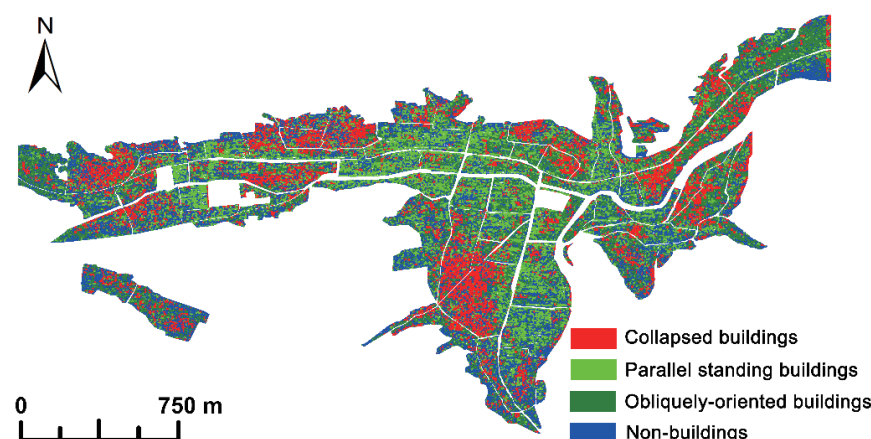


Fig. 9. (Color online) Extraction results of the three post-earthquake building types in Yushu County.

Table 2

Confusion matrix for accuracy assessment of recognition results of three types of buildings.

	Experiment		
	Collapsed buildings	Obliquely oriented buildings (No. of samples)	Parallel standing buildings
Reference			
Collapsed buildings	20266	4734	0
Obliquely oriented buildings	7456	17544	0
Parallel standing buildings	1209	625	23166
Overall accuracy: 81.30%			

5. Discussion

There are some recognized collapsed buildings with an orderly and regular distribution at the image boundary in the upper right corner of Fig. 9. This is because the SPAN image needs to be replenished to adapt to the size of the calculation window when calculating STFFAS, which is known as the boundary supplement effect. As seen in Table 2, when using the proposed method to extract building earthquake damage information, the producer's accuracy (PA) of damaged buildings, which is the correct recognition rate of collapsed buildings, is 81.06%; and the PA of undamaged buildings, which is the correct recognition rate of obliquely oriented and parallel standing buildings, reaches 81.42%. That is, the PA of both damaged and undamaged buildings is above 80%, showing that the recognition of damaged and undamaged buildings is relatively balanced without an underestimation of undamaged buildings caused by the overestimation of damaged buildings or vice versa. Therefore, the recognition results of the proposed method are reliable for post-earthquake building damage assessment and support safety, because the overrecognition of damaged buildings will lead to a waste of rescue resources, while the underrecognition of damaged buildings will delay the rescue of buried people, increasing the danger to them.

On the basis of the correct recognition rate of obliquely oriented buildings, 70.18% of the obliquely oriented buildings were separated from the volume scattering components. If such obliquely oriented buildings are misclassified as collapsed buildings, much manpower and material resources will be misdirected. By the Y4O method, all ground objects whose dominant scattering component is the volume scattering components will be classified as collapsed buildings. Although this method can achieve a recognition rate of 100% for collapsed buildings, the correct recognition rate of undamaged buildings is only 46.33%, i.e. $23166/(25000 + 25000) \approx 46.33\%$. Therefore, when using the Y4O method to recognize building earthquake damage, the inaccurate classification of the volume scattering components will cause an immoderate sacrifice of the correct recognition rate of undamaged buildings in exchange for the correct recognition rate of collapsed buildings.

Most of the misclassified collapsed and obliquely oriented buildings appear at the junction or boundary of two ground objects owing to the square calculation window. A calculation window may contain multiple ground objects and many rows and columns. The junction of different objects is often only 1 or 2 pixels wide. Then, the calculation window will have a smoothing effect at this boundary, so the two different objects at the junction will be recognized as one object. Parallel standing buildings are misclassified as collapsed and obliquely oriented buildings mainly because some roof areas and transition zones between overlaying and shadow have lower scattering intensities. As a result, the parallel standing buildings with weaker scattering intensity are misclassified as collapsed and obliquely oriented buildings. In addition, errors in the manual selection of verification samples may lead to the misclassification of the three types of buildings, e.g., other ground object samples that do not belong to the verification sample category may be sporadically distributed in a complete verification sample zone. In other cases, the edges of selected building samples may be prone to mixing with other ground objects.

Since the STFFAS values of the obliquely oriented buildings are greater than those of the collapsed buildings, the larger the STFFAS segmentation threshold value is, the more collapsed buildings are recognized and the more collapsed buildings are misrecognized as obliquely oriented buildings. This will result in an overestimation of collapsed buildings and an underestimation of standing buildings. Conversely, the smaller the STFFAS segmentation threshold value is, the fewer collapsed buildings are recognized and the easier it becomes for damaged buildings to not be recognized, which may delay rescue operations and cause great risks to emergency rescue. Therefore, the segmentation threshold value of STFFAS for obliquely oriented and collapsed buildings cannot be set too small to obtain a high recognition accuracy of obliquely oriented buildings. It should be appropriately set on the premise that the correct recognition rate of collapsed buildings is not less than 80%, so as to ensure that the correct recognition rate of obliquely oriented buildings will be above 80%.

6. Conclusions

To solve the problem of the overclassification of collapsed buildings when using the Y4O method, in this paper, we proposed a parameter called STFFAS that can describe the texture features for the amplitude spectrum of the frequency domain from Fourier transform. STFFAS proposed herein can be used to better distinguish between collapsed and obliquely oriented buildings, which present similar scattering intensities and are dominated by the same scattering component in the SAR image. STFFAS well differentiates the spatial textures of collapsed and obliquely oriented buildings on the basis of the frequency-domain properties. Therefore, we proposed to use STFFAS to process a large number of obliquely oriented buildings mixed amongst the collapsed buildings recognized by the Y4R method in order to improve the recognition accuracy of building earthquake damage. The STFFAS image corresponding to the SPAN image of PolSAR data was calculated. The volume scattering components obtained from the PolSAR data by the Y4R method were segmented using the STFFAS values and further divided into collapsed and obliquely oriented buildings. The overrecognition of disasters by directly classifying all the volume scattering components obtained by the Y4O method into collapsed buildings has been significantly alleviated. The experimental results also show that the proposed method for extracting building earthquake damage information can better recognize the damaged and undamaged buildings in the earthquake-stricken area, and hence attain a relatively high recognition accuracy of building earthquake damage. 70.18% of obliquely oriented buildings were successfully separated from the collapsed buildings recognized by the Y4R method, which has significantly improved the extraction accuracy of building earthquake damage information. Because of limitations in our data, no further experimental data were available for our experiment in this study. We will further verify the robustness of the proposed method when other relevant earthquake data are obtained. In addition, we will conduct in-depth research on the selection of segmentation thresholds to reduce artificial errors.

Acknowledgments

This work was supported by the Gansu Earthquake Administration Innovation Team Special Fund, grant number 2019TD-01-02; the National Natural Science Foundation of China, grant number 42371404 and 41601479; the Gansu Province Science and Technology Program, grant number 22JR5RA822; the Key Talent Project of Gansu Province, grant number 11276679015; the Basic Research Project of Institute of Earthquake Forecasting, China Earthquake Administration, grant number 2021IESLZ4; the State Scholarship Fund of China Scholarship Council (CSC); and the Science for Earthquake Resilience of China Earthquake Administration, grant number XH18049.

References

- 1 W. Zhai, H. F. Shen, C. L. Huang, and W. S. Pei: Proc. 2016 IEEE Int. Geoscience and Remote Sensing Symp. (IEEE, 2016) 7338–7341. <https://doi.org/10.1109/IGARSS.2016.7730914>
- 2 W. Zhai, C. L. Huang, W. S. Pei, and Y. Li: Proc. 2017 IEEE Int. Geoscience and Remote Sensing Symp. (IEEE, 2017) 1036–1039. <https://doi.org/10.1109/IGARSS.2017.8127132>
- 3 W. Zhai, X. Q. Wang, Y. X. Bi, G. Y. Zhu, and J. Q. Du: *Sens. Mater.* **34** (2022) 12. <https://doi.org/10.18494/SAM4188>
- 4 W. Zhai and C. L. Huang: *Earth Planets Space* **68** (2016) 86. <https://doi.org/10.1186/s40623-016-0469-2>
- 5 P. Mazzanti, S. Scancella, M. Virelli, S. Frittelli, V. Nocente, and F. Lombardo: *Remote Sens.* **14** (2022) 19. <https://doi.org/10.3390/rs14092210>
- 6 C. Wang, H. Zhang, F. Wu, B. Zhang, Y. X. Tang, H. A. Wu, X. Y. Wen, and D. M. Yan: *J. Appl. Remote Sens.* **3** (2009) 1. <https://doi.org/10.1117/1.3154558>
- 7 X. W. Li, H. D. Guo, L. Zhang, X. Chen, and L. Liang: *IEEE Geosci. Remote Sens. Lett.* **9** (2012) 4. <https://doi.org/10.1109/LGRS.2011.2178392>
- 8 Q. H. Chen, L. L. Li, P. Jiang, and X. G. Liu: Proc. 2016 IEEE Int. Geoscience and Remote Sensing Symp. (IEEE, 2016) 5769–5772. <https://doi.org/10.1109/IGARSS.2016.7730507>
- 9 W. Zhai, H. F. Shen, C. L. Huang, and W. S. Pei: *Remote Sens.* **8** (2016) 3. <https://doi.org/10.3390/rs8030171>
- 10 Y. Q. Ji, T. S. S. Josaphat, M. Y. Chua, and M. M. Waqar: *Remote Sens.* **10** (2018) 7. <https://doi.org/10.3390/rs10071088>
- 11 W. Zhai, C. L. Huang, and Pei W.S.: *Remote Sens.* **10** (2018) 10. <https://doi.org/10.3390/rs10101613>
- 12 S. Liu, F. L. Zhang, S. Y. Wei, Q. B. Liu, N. Liu, Y. Shao, and S. J. Burian: *Front. Earth Sci.* **14** (2020) 2. <https://doi.org/10.1007/s11707-019-0779-3>
- 13 W. Zhai, J. F. Zhang, X. L. Xiao, J. H. Wang, H. R. Zhang, X. X. Yin, and Z. Wu: *Remote Sens. Lett.* **12** (2021) 6. <https://doi.org/10.1080/2150704X.2021.1906975>
- 14 H. Miao, X. Q. Wang, L. Ding, X. Ding: Proc. 2021 IEEE Int. Geoscience and Remote Sensing Symp. IGARSS (IEEE, 2021) 8566–8569. <https://doi.org/10.1109/IGARSS47720.2021.9555084>
- 15 Y. L. Nie, Q. M. Zeng, H. Z. Zhang, and Q. Wang: *Remote Sens.* **13** (2021) 6. <https://doi.org/10.3390/rs13061146>
- 16 Y. B. Bai, B. Adriano, E. Mas, and S. Koshimura: *J. Disaster Res.* **13** (2018) 2. <https://doi.org/10.20965/jdr.2018.p0291>
- 17 L. L. Li, X. G. Liu, Q. H. Chen, and S. Yang: *Comput. Geosci-UK.* **113** (2018) 115. <https://doi.org/10.1016/j.cageo.2018.01.018>
- 18 W. Zhai, C. L. Huang, and W. S. Pei: *Remote Sens.* **11** (2019) 8. <https://doi.org/10.3390/rs11080897>
- 19 Q. H. Chen, H. Yang, L. L. Li, and X. G. Liu: *IEEE J. of Sel. Top. Appl. Earth Obs. Remote Sens.* **13** (2020) 154. <https://doi.org/10.1109/JSTARS.2019.2954292>
- 20 D. Hu, J. J. Chen, and S. Li: *Automat. Constr.* **140** (2022) 104380. <https://doi.org/10.1016/j.autcon.2022.104380>
- 21 D. D. Acula: *Acta Manilana* **70** (2022) 13. <https://doi.org/10.53603/actamanil.70.2022.wpyl1791>
- 22 Y. F. Da, Z. Y. Ji, Y. S. Zhou: *Mathematics* **10** (2022) 1898. <https://doi.org/10.3390/math10111898>
- 23 S. T. Seydi, H. Rastiveis, B. Kalantar, A. A. Halin, and N. Ueda: *Remote Sens.* **14** (2022) 9. <https://doi.org/10.3390/rs14092214>
- 24 Y. Yamaguchi, A. Sato, W. M. Boerner, R. Sato, and H. Yamada: *IEEE Trans. Geosci. Remote Sens.* **49** (2011) 6. <https://doi.org/10.1109/TGRS.2010.2099124>
- 25 J. W. Cooley, P. A. W. Lewis, and P. D. Welch: *IEEE Trans. Educ.* **12** (1969) 1. <https://doi.org/10.1109/TE.1969.4320436>